Influence of Resonance on the Acidity of Sulfides, Sulfoxides, Sulfones, and Their Group 16 Congeners

Eric D. Glendening* and Anthony L. Shrout†

Department of Chemistry, Indiana State University, Terre Haute, Indiana 47809

Received: January 11, 2005; In Final Form: March 28, 2005

The influence of resonance on the acidities of dimethyl sulfide (DMS), dimethyl sulfoxide (DMSO), and dimethyl sulfone ($DMSO_2$) and their group 16 congeners ($DMXO_n$ for X = Se, Te, Po and $n = 0-2$) is examined using ab initio methods and the natural bond orbital (NBO) and natural resonance theory (NRT) analyses. Gas-phase acidities are evaluated using B3LYP-optimized geometries with coupled cluster energies and complete basis set extrapolation. The acidity of the $DMSO_n$ molecules increases with increasing coordination of the central S atom. Acidity also tends to increase when the central atom is substituted by a heavier group 16 atom. NRT analysis reveals significant resonance delocalization in the $DMXO_n$ molecules and their anions. On deprotonation, the $DMXO_n$ molecules undergo structural changes that are consistent with changes in the resonance character of the calculated charge densities. However, resonance cannot account for the trends in the deprotonation energies. Whereas the DMX^- anions are more strongly resonance stabilized than their parent molecules DM*X*, the $DMXO_2^-$ anions and $DMXO_2$ molecules are nearly equally resonance stabilized. Thus, there appears to be no extra stabilization of $DMXO_2^-$ compared to that of DMX^- that would account for the enhanced acidity of $DMXO_2$ relative to DM*X*.

I. Introduction

Dimethyl sulfide (DMS) is a weaker acid than dimethyl sulfoxide (DMSO), which, in turn, is a weaker acid than dimethyl sulfone ($DMSO_2$). This acidity trend is most generally understood based on the stability of the carbanions that result on deprotonation, the strongest acid corresponding to the most stable anion. A number of mechanisms have been proposed to account for the varying stabilities of these anions, including resonance delocalization and electrical interactions (polarization). Resonance stabilization of the anions of DMS, DMSO, and $DMSO_2$ is understood to strengthen as the charge at the anionic carbon increasingly delocalizes on to the respective methylsulfenyl (SCH_3), methylsulfinyl ($SOCH_3$), and methylsulfonyl (SO_2CH_3) groups.[1] Substantial theoretical evidence suggests, however, that classical electrical interactions may more importantly impact the acidity trend.[2] Carbanions are stabilized when bonded to heteroatoms, an effect that has been attributed to the greater polarizability of these atoms relative to that of C.[3−8] Moreover, the oxidation state of the central S atom formally increases in the $DMSO_n$ series with increasing n as O atoms withdraw electron density, resulting in a more strongly, positively charged heteroatom that stabilizes the carbanion center through electrostatic interaction. One would argue, then, that $DMSO_2$ is the strongest acid in the series because the S center in the $DMSO_2$ anion (which we will denote $DMSO_2^-$) carries the largest positive charge and, therefore, stabilizes its carbanion center more strongly than that of the DMS and DMSO anions.

Our interest in the acidity of the $DMSO_n$ molecules regards the role of resonance stabilization because conflicting conclusions regarding the extent of resonance in these molecules have been reported. Based on an evaluation of atomic charges using the atoms in molecules (AIM) method,[9] Speers et al.[2] concluded that the negative charge of the anions remains largely localized on the methylene group as the coordination of the central S atom increases. Charge relaxation effects in the anions also diminished with increasing coordination, leading Speers et al. to judge that resonance stabilization of the anions is unimportant. However, Wiberg and Castejon,[1] also using the AIM method, calculated that the negative charge on the methylene group decreased significantly with increasing coordination of the central atom. Based on these results and trends in the calculated rotation barriers and covalent bond orders, Wiberg and Castejon argued that resonance is indeed important in stabilizing the anions.

The influence of resonance on the acidity trend in the $DMSO_n$ molecules remains unclear and deserves further investigation. We use the natural bond orbital (NBO)[10] and natural resonance theory (NRT)[11] methods in this work to determine quantitatively the extent of resonance delocalization in the $DMSO_n$ molecules and their anions and the degree to which delocalization impacts deprotonation. NBO and NRT are localized orbital methods, unlike AIM, that facilitate the identification of delocalizing orbital interactions, resonance hybrids, and bond orders and the determination of their influence on the molecular structure and acidity trend. We also examine in this work the acidity trends for the group 16 congeners, $DMXO_n$ (X = Se, Te, Po and $n = 0-2$).

II. Calculations

Geometry optimizations were performed with Gaussian 98[12] using density functional theory (specifically the B3LYP hybrid functional[13]) and polarized, double-ζ quality basis sets. Dunning's correlation consistent aug-cc-pVDZ basis sets[14] were used for all H, C, O, and S atoms. Peterson's all-electron aug-cc-pVDZ set for Se and valence aug-cc-pVDZ-PP sets for Te and

* Corresponding author E-mail: glendening@indstate.edu.
† Present address: Department of Chemistry, University of Massachusetts, Amherst, MA, 01003.

10.1021/jp058010f CCC: $30.25
Published on Web 05/17/2005

TABLE 1: Optimized Structural Parameters of the $DMXO_n$ Molecules (X = S, Se, Te, Po; n = 0−2) and Their Anions[a]

	$X-C_\alpha$	$X-CH_3$	$X-O$	$C_\alpha-X-CH_3$	$C_\alpha-X-O$
DMS	1.829	1.829		99.50	
DMS^-	1.747	1.912		110.66	
DMSe	1.970	1.970		96.95	
$DMSe^-$	1.887	2.073		110.79	
DMTe	2.178	2.178		94.30	
$DMTe^-$	2.090	2.292		112.07	
DMPo	2.286	2.286		93.27	
$DMPo^-$	2.220	2.406		112.69	
DMSO	1.841	1.841	1.540	96.86	106.02
$DMSO^-$	1.739	1.850	1.592	98.69	117.97
DMSeO	1.982	1.982	1.680	94.58	103.84
$DMSeO^-$	1.884	1.991	1.732	96.21	117.57
DMTeO	2.180	2.180	1.857	91.77	101.97
$DMTeO^-$	2.076	2.196	1.908	93.70	118.22
DMPoO	2.292	2.292	1.963	91.06	100.48
$DMPoO^-$	2.213	2.308	2.017	92.53	117.45
$DMSO_2$	1.817	1.817	1.494	104.21	107.77
$DMSO_2^-$	1.700	1.869	1.520	113.76	110.86
$DMSeO_2$	1.956	1.956	1.645	103.89	107.59
$DMSeO_2^-$	1.875	1.973	1.677	105.56	114.30
$DMTeO_2$	2.155	2.155	1.835	102.42	107.49
$DMTeO_2^-$	2.084	2.168	1.866	103.46	115.76
$DMPoO_2$	2.286	2.286	1.955	102.20	107.35
$DMPoO_2^-$	2.265	2.290	1.986	101.86	117.04

[a] B3LYP/aVDZ optimized values. All bond lengths are given in Å and bond angles in degrees. C_α is the anionic carbon in the anions. The structural parameters for the $DMXO_2^-$ molecules are for the equilibrium antiperiplanar (X = S) and synperiplanar (X = Se, Te, and Po) conformations.

Po were used, the latter with small-core pseudo-potentials.[15] We use the abbreviation aVDZ to represent these double-ζ sets. The equilibrium character of each optimized geometry was confirmed by Gaussian 98 frequency calculations. B3LYP/aVDZ optimized structural parameters are listed in Table 1.

Table 2 lists the B3LYP/aVDZ deprotonation energies, ΔE, corresponding to the reactions

$$DMXO_n \rightarrow H^+ + DMXO_n^- \ (X = \text{S, Se, Te, Po; } n = 0\text{-}2) \quad (1)$$

Coupled cluster energy evaluations, at the CCSD(T) level, were performed with MOLPRO[16] at the B3LYP/aVDZ optimized geometries. Energies at the complete basis set (CBS) limit were then estimated by extrapolating the CCSD(T) energies using the fitting function[17]

$$E_n = E_{CBS} + Ae^{-(n-1)} + Be^{-(n-1)^2} \quad (2)$$

with the correlation consistent family of basis sets, aug-cc-pVnZ (H, C, O, S, Se) and aug-cc-pVnZ-PP (Te, Po), where n represents the cardinal number of the basis set (2 for double-ζ, 3 for triple-ζ, and 4 for quadruple-ζ). In eq 2, E_n is the CCSD(T) energy evaluated with the nth basis set and A, B, and E_{CBS} are fitting parameters, the latter corresponding to the estimated CCSD(T)/CBS limiting energy. Reaction enthalpies and free energies at 298 K were evaluated using standard statistical mechanical expressions for zero-point energies, thermal corrections, and entropies. B3LYP vibrational frequencies were scaled by the usual factor, 0.96. Table 2 reports calculated deprotonation enthalpies and free energies with comparison values for the $DMSO_n$ molecules from experiment.[18,19]

Resonance descriptions of the $DMXO_n$ molecules and anions were obtained using natural resonance theory (NRT).[11] NRT is a density-based approach to resonance theory implemented in the natural bond orbital (NBO) program.[10] NRT expands the total density operator, $\hat{\Gamma}$, as a sum of operators (a resonance hybrid)

$$\hat{\Gamma} \cong \sum_\alpha w_\alpha \hat{\Gamma}_\alpha \quad (3)$$

where $\hat{\Gamma}_\alpha$ represents the idealized density of the resonance structure α. The optimized weights w_α of this expansion are subject to positivity and normalization conditions

$$w_\alpha \geq 0, \quad \sum_\alpha w_\alpha = 1 \quad (4)$$

Fractional bond orders are closely related to the ideas of resonance structures and weights. The natural bond order, b_{AB}, of a resonance hybrid is defined by

$$b_{AB} = \sum_\alpha w_\alpha b_{AB}^\alpha \quad (5)$$

where b_{AB}^α represents the integer number of bonds between atoms A and B in the αth structure. The values obtained for the weights w_α and bond orders b_{AB} are based solely on the optimal representation of the total electron density as a resonance expansion of idealized densities. Note that the NRT method polarizes the bonds of its resonance structures to best describe the charge distribution. Thus, separate covalent and ionic structures are not required to represent bond polarization. In the present study, we used single-reference NRT with a second-order energy threshold (NRTTHR) of 0.5 kcal/mol.

The energy of the leading resonance (Lewis) structure of each resonance hybrid was determined using NBO energetic analysis. The NBO method calculates a set of localized one- and two-center orbitals representing the Lewis structure of the system. Fractional occupancies of the non-Lewis orbitals (principally the antibonds) stem from delocalizing (resonance) interactions with the Lewis orbitals (the bonds and lone pairs). Density is localized in the Lewis orbitals by setting to zero all elements of the Kohn−Sham matrix that couple Lewis with non-Lewis orbitals. The eigenvectors of this modified Kohn−Sham matrix give a localized density distribution in which each Lewis orbital is doubly occupied. A single pass of the localized density through the self-consistent field routines, then, yields the energy of the Lewis structure. Equilibrium geometries for these localized systems were fully optimized using the numerical Fletcher-Powell algorithm of Gaussian 98. Directed NBO search (CHOOSE) and a reduced occupancy threshold (THRESH = 1.8) were used to ensure numerical stability during the optimizations.

III. Molecular Structure and Acidity Trend

Table 1 lists selected structural parameters for the $DMXO_n$ molecules and their anions. The most stable conformations of the $DMXO_n$ molecules have qualitatively similar structural features. All bonds are staggered in the minimum energy forms and the geometries at the central X atoms are bent (DMX), pyramidal ($DMXO$), or approximately tetrahedral ($DMXO_2$). Deprotonation yields $DMXO_n^-$ anions that likewise have similar structural characteristics. The lone pairs of the anionic C_α centers are oriented antiperiplanar to the CH_3 groups in DMX^- (**1**), antiperiplanar to the O atom in $DMXO^-$ (**2**), and either antiperiplanar (**3**) or synperiplanar (**4**) to the CH_3 group in $DMXO_2^-$. The two conformations of $DMSO_2^-$ are nearly isoenergetic, with **3** slightly (by 0.5 kcal/mol) more stable than

TABLE 2: Gas-Phase Acidities of DM*X*O$_n$ (*X* = S, Se, Te, Po; *n* = 0−2)[a]

	B3LYP/aVDZ ΔE	CCSD(T)/CBS ΔE	CCSD(T)/CBS ΔH	CCSD(T)/CBS ΔG	ΔH(expt)	ΔG(expt)
DMS	400	402	394	386	393 ± 2[b]	386 ± 2[b]
DMSe	397	400	392	384		
DMTe	393	395	387	379		
DMPo	393	395	388	380		
DMSO	382	384	376	369	374 ± 2[c]	367 ± 2[c]
DMSeO	381	382	375	368		
DMTeO	379	380	373	366		
DMPoO	381	382	375	368		
$DMSO_2$	373	376	368	360	366 ± 3[c]	359 ± 2[c]
$DMSeO_2$	366	369	361	353		
$DMTeO_2$	360	363	354	347		
$DMPoO_2$	356	360	350	343		

[a] All values in kcal/mol for eq 1 at B3LYP/aVDZ optimized geometries. ΔH and ΔG values are at 298 K. [b] Reference 18. [c] Reference 19.

4 at the CCSD(T)/CBS level. For the Se, Te, and Po congeners, **4** is more stable than **3** by 1.1, 1.8, and 2.9 kcal/mol, respectively.

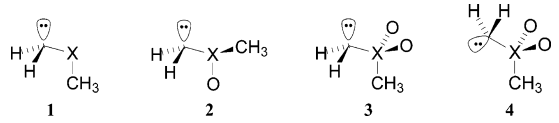

1 **2** **3** **4**

The bond lengths and angles at the central atom undergo significant changes upon deprotonation. The *X*−CH_2 bond lengths decrease, whereas the *X*−CH_3 and *X*−O distances increase, and the C−*X*−C and C−*X*−O angles increase. For example, in DMS, deprotonation shortens the S−CH_2 bond by ca. 0.08 Å, whereas the S−CH_3 bond lengthens by roughly 0.08 Å. The C−S−C bond angle opens considerably, by nearly 11°. For DMSO, the S−CH_2 bond shortens by nearly 0.10 Å, whereas the S−CH_3 and S−O bonds lengthen by only 0.01 and 0.05 Å, respectively. We return to the structural features of the DM*X*O$_n$ molecules and their anions in the following section where we consider the role of resonance delocalization.

Gas-phase deprotonation energies, enthalpies, and free energies are reported in Table 2. The enthalpy and free energy values were obtained by applying B3LYP/aVDZ zero-point energy, thermal, and entropic corrections to the CCSD(T)/CBS energies. In general, we find that the B3LYP functional with a double-ζ basis set yields reasonably accurate estimates of the deprotonation energies. The B3LYP/aVDZ ΔE values are typically 1−3 kcal/mol (0.2−0.7%) weaker than the respective CCSD(T)/CBS energies. The calculated ΔH and ΔG values for the $DMSO_n$ molecules are in excellent agreement with experimental determinations, lying within estimated error bounds. B3LYP/aVDZ level calculations thus compare favorably with experiment and with higher level calculations. Throughout the remainder of this work, we will focus on trends observed in the B3LYP/aVDZ energies.

Two trends are apparent in the data of Table 2. The more significant of these relates to the increasing coordination of the central atom by O atoms. Increasing coordination enhances acidity by decreasing the deprotonation energy. Thus, ΔE decreases from 400 kcal/mol for DMS to 382 and 373 kcal/mol for DMSO and $DMSO_2$, respectively. The Se, Te, and Po congeners exhibit similar trends. A less significant trend is associated with the substitution of the central atom by a heavier group 16 atom. Such substitution generally decreases ΔE somewhat, again enhancing acidity. Thus, the deprotonation energies of the DM*X*O_2 molecules decrease from 373 (S) to 368 (Se), 362 (Te), and 359 (Po) kcal/mol. Similar trends of comparable magnitudes are observed in the enthalpies and free energies.

TABLE 3: NRT Analysis of the DM*X*O$_n$ Molecules (*X* = S, Se, Te, Po; *n* = 0−2)[a]

	CH_3-X-CH_3		
DMS	95.1		
DMSe	96.3		
DMTe	97.0		
DMPo	98.0		
	$CH_3-\overset{O}{\underset{|}{X}}-CH_3$	$CH_3-\overset{O}{\underset{\|}{X}}\ CH_3$ $n_O \rightarrow \sigma^*_{XC}$	
DMSO	84.1	5.5 (2)	
DMSeO	85.3	5.7 (2)	
DMTeO	86.8	5.6 (2)	
DMPoO	87.7	5.4 (2)	
	$CH_3-\overset{O}{\underset{O}{\underset{|}{X}}}-CH_3$	$CH_3-\overset{O}{\underset{O}{\underset{|}{\overset{\|}{X}}}}\ CH_3$ $n_O \rightarrow \sigma^*_{XC}$	$CH_3-\overset{O}{\underset{O}{\underset{|}{X}}}-CH_3$ $n_O \rightarrow \sigma^*_{XO}$
$DMSO_2$	60.9	4.5 (4)	7.4 (2)
$DMSeO_2$	61.3	4.2 (4)	7.1 (2)
$DMTeO_2$	62.5	3.1 (4)	7.2 (2)
$DMPoO_2$	59.4	5.0 (4)	4.2 (2)

[a] B3LYP/aVDZ percentage weights. Values in parentheses indicate the number of structures of this type that contribute to the resonance hybrid. Lone pairs and formal charges are omitted for clarity in all structures; the octet rule is satisfied at every heavy atom.

IV. Resonance and Molecular Structure

The DM*X*O$_n$ molecules undergo, on deprotonation, significant structural changes that are conventionally understood to arise from the resonance delocalization of the resulting anions. We consider here the resonance descriptions of the DM*X*O$_n$ molecules and their anions and their relationship to molecular structure. Tables 3 and 4 report the results of NRT analysis.

Resonance hybrids for the DM*X*O$_n$ molecules are generally dominated by single Lewis structures but include weaker contributions from secondary forms associated with delocalizing orbital interactions. Table 3 lists the primary structure for each molecule together with the leading secondary forms. For example, NRT analysis of DMS yields a hybrid comprised of nine structures. The primary structure, at 95.1%, is the usual Lewis form exhibiting a pair of S−C single bonds. Weak hyperconjugative interactions give rise to the additional eight secondary structures (not shown), none of which contributes more than 1%. The DMSO hybrid consists of 19 structures, of which three are shown. The primary structure contributes 84.1%, and two double bond−no bond forms, stemming from strong delocalization of O nonbonding electrons into vicinal S−C antibonds ($n_O \rightarrow \sigma^*_{SC}$), each contribute an additional 5.5%.

TABLE 4: NRT Analysis of the $DMXO_n$ Anions (X = S, Se, Te, Po; n = 0−2)[a]

	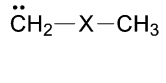 $n_C \rightarrow \sigma^*_{XC}$	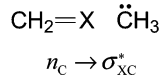 $n_C \rightarrow \sigma^*_{XC}$	$n_C \rightarrow \sigma^*_{XO}$	$n_O \rightarrow \sigma^*_{XC}$	$n_O \rightarrow \sigma^*_{XC}$	$n_O \rightarrow \sigma^*_{XO}$
DMS^-	83.9	9.7				
$DMSe^-$	84.3	10.7				
$DMTe^-$	84.9	12.1				
$DMPo^-$	86.2	11.4				
	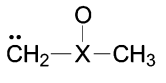	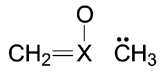 $n_C \rightarrow \sigma^*_{XC}$	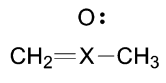 $n_C \rightarrow \sigma^*_{XO}$	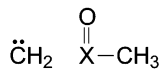 $n_O \rightarrow \sigma^*_{XC}$	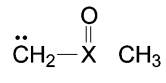 $n_O \rightarrow \sigma^*_{XC}$	
$DMSO^-$	77.3	1.3	8.0	4.1	4.6	
$DMSeO^-$	77.8	1.2	8.2	4.0	4.5	
$DMTeO^-$	77.2	2.0	8.4	4.4	4.7	
$DMPoO^-$	79.5	1.5	6.9	4.0	4.6	
	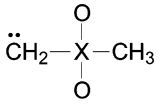	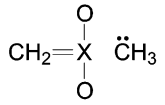 $n_C \rightarrow \sigma^*_{XC}$	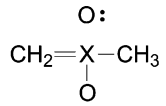 $n_C \rightarrow \sigma^*_{XO}$	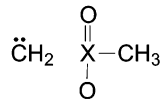 $n_O \rightarrow \sigma^*_{XC}$	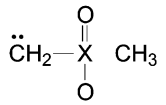 $n_O \rightarrow \sigma^*_{XC}$	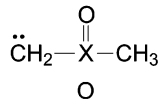 $n_O \rightarrow \sigma^*_{XO}$
$DMSO_2^-$	59.5	8.1	<0.1 (2)	3.1 (2)	0.8 (2)	9.4 (2)
$DMSeO_2^-$	60.3	3.9	1.8 (2)	2.9 (2)	2.6 (2)	6.4 (2)
$DMTeO_2^-$	59.4	7.7	<0.1 (2)	2.7 (2)	1.7 (2)	6.7 (2)
$DMPoO_2^-$	56.6	4.2	0.9 (2)	2.1 (2)	2.5 (2)	5.2 (2)

[a] B3LYP/aVDZ percentage weights. Values in parentheses indicate the number of structures of this type that contribute to the resonance hybrid. The only nonbonding electron pair shown is that originating from the carbanion center in the parent Lewis structure; all other nonbonding pairs and all formal charges are omitted for clarity. The octet rule is satisfied at every heavy atom.

Seven structures contribute importantly in $DMSO_2$, including the Lewis form (60.9%), four structures resulting from $n_O \rightarrow \sigma^*_{SC}$ interactions (4.5% each), and two structures resulting from $n_O \rightarrow \sigma^*_{SO}$ interactions (7.4% each). Table 3 clearly reveals the increasing extent of delocalization in the $DMXO_n$ molecules with increasing coordination of the central atom. The DMX molecules are highly localized, each well described by a single Lewis structure having a weight in excess of 95%. In contrast, the $DMXO_2$ molecules are fairly strongly delocalized, the Lewis structure contributing only about 60% of the resonance hybrid.

NRT analysis of the $DMXO_n^-$ anions is reported in Table 4. Of particular interest is the extent to which deprotonation enhances the delocalization in these systems. We find that the DMX^- anions are significantly more strongly delocalized than the parent molecules. For example, the weight of the primary structure falls from 95.1% in DMS to 83.9% in DMS^- as a secondary structure arising from negative hyperconjugation of the C nonbonding electrons ($n_C \rightarrow \sigma^*_{SC}$) contributes 9.7% to the latter. The $DMXO^-$ anions are likewise somewhat more delocalized than their parent molecules. The contribution of the primary structure decreases from 84.1% in DMSO to 77.3% in $DMSO^-$ as a double bond−no bond structure arising from the $n_C \rightarrow \sigma^*_{SO}$ interaction gains considerable (8.0%) weight. Interestingly, however, it appears that the $DMXO_2$ and $DMXO_2^-$ systems are roughly equally delocalized. Whereas the conventional resonance description would suggest increased delocalization in the anion, NRT reveals primary structures for the $DMSO_2$ and $DMSO_2^-$ hybrids of nearly equal weight, 60.9% and 59.5%, respectively. A secondary structure stemming from $n_C \rightarrow \sigma^*_{SC}$ delocalization clearly contributes to the anion (8.1%), but apparently at the expense of the strong $n_O \rightarrow \sigma^*_{SC}$ interactions present in the parent molecule. The total weight of the four $n_O \rightarrow \sigma^*_{SC}$ resonance forms falls from 18.0% in $DMSO_2$ to 7.8% in $DMSO_2^-$. NRT analysis therefore suggests that deprotonation significantly increases the extent of delocalization in the DMX molecules, moderately increases the delocalization of $DMXO$, and has limited influence on the degree of delocalization in $DMXO_2$.

Natural bond orders were evaluated for each equilibrium structure. Results are given in Table 5. DMS is well described by a single Lewis structure that exhibits S−C single bonds. The calculated S−C bond orders, 1.016, for this molecule thus differ only marginally from unit values. (The slight deviation of these values from 1.000 arises from weak $n_S \rightarrow \sigma^*_{CH}$ hyperconjugative interactions that contribute a minor amount of S−C double bond character.) A double bond−no bond resonance form contributes importantly in DMS^-, as shown in Table 4. The $S-CH_2$ bond order thereby increases to 1.113, whereas the $S-CH_3$ bond order decreases to 0.920, consistent with the shortened and lengthened bond lengths. The bond orders for the other molecules, and their changes upon deprotonation, can similarly be understood based on the character of the resonance hybrids of Tables 3 and 4.

Of particular interest in this work is the degree to which the bond length changes the $DMXO_n$ molecules undergo on deprotonation can be rationalized based on the character of the resonance hybrids. Naturally, therefore, we seek to understand the correlation of equilibrium bond lengths with bond order. Figure 1 plots optimized S−C bond lengths vs natural bond order for the S-containing molecules. Three linear, and nearly parallel, correlations are observed, one for the sulfides DMS/DMS^- (circles), a second for the sulfoxides DMSO/$DMSO^-$ (squares), and a third for the sulfones $DMSO_2$/$DMSO_2^-$ (diamonds). Bond length−bond order plots were also prepared

TABLE 5: Natural Bond Orders of the $DMXO_n$ Molecules (X = S, Se, Te, Po; n = 0−2) and Their Anions[a]

	$X-C_\alpha$	$X-CH_3$	$X-O$
DMS	1.016	1.016	
DMS^-	1.113	0.920	
DMSe	1.011	1.011	
$DMSe^-$	1.117	0.902	
DMTe	1.008	1.008	
$DMTe^-$	1.125	0.884	
DMPo	1.006	1.006	
$DMPo^-$	1.113	0.887	
DMSO	0.953	0.953	1.097
$DMSO^-$	1.067	0.943	1.007
DMSeO	0.950	0.950	1.096
$DMSeO^-$	1.060	0.939	0.999
DMTeO	0.943	0.943	1.097
$DMTeO^-$	1.061	0.932	0.999
DMPoO	0.944	0.944	1.096
$DMPoO^-$	1.039	0.928	0.998
$DMSO_2$	0.911	0.911	1.081
$DMSO_2^-$	1.033	0.875	1.037
$DMSeO_2$	0.909	0.909	1.063
$DMSeO_2^-$	1.004	0.880	1.010
$DMTeO_2$	0.882	0.882	1.030
$DMTeO_2^-$	0.979	0.878	0.989
$DMPoO_2$	0.857	0.857	0.977
$DMPoO_2^-$	0.909	0.864	0.948

[a] B3LYP/aVDZ optimized values. C_α is the anionic carbon in the anions.

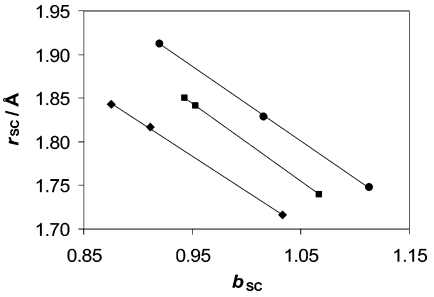

Figure 1. Plot of equilibrium S−C bond length vs natural bond order for DMS/DMS^- (circles), DMSO/$DMSO^-$ (squares), and $DMSO_2$/$DMSO_2^-$ (diamonds).

for the Se-, Te-, and Po-containing molecules (not shown). Similar, nearly linear correlations were observed in all cases. Although resonance accounts for changes in structure for a single system (e.g., DMS to DMS^-), it apparently cannot be used alone to predict absolute bond lengths for all systems considered here.

Equilibrium bond lengths $r_{AB}^{(eq)}$ can be considered to result from two effects, Lewis and non-Lewis

$$r_{AB}^{(eq)} = r_{AB}^{(Lewis)} + \Delta r_{AB}^{(non-Lewis)} \quad (6)$$

Every bond has an idealized length, $r_{AB}^{(Lewis)}$, that principally depends on the hybridizations of the orbitals that comprise the localized Lewis structure. Non-Lewis (resonance) effects then cause the bond to stretch or contract by $\Delta r_{AB}^{(non-Lewis)}$ according to the type and strength of the delocalizing interactions in the molecule. Note that natural bond orders b_{AB} are based on the character of the resonance hybrids (cf Tables 3 and 4) and, therefore, account for non-Lewis effects but neglect the role of hybridization. Thus, one should not necessarily anticipate strong correlation of bond order with absolute bond length $r_{AB}^{(eq)}$. Rather, one may instead find that natural bond order correlates more directly with bond length variation $\Delta r_{AB}^{(non-Lewis)}$.

The idealized bond length $r_{AB}^{(Lewis)}$ corresponds to the distance between atoms A and B if the bond order b_{AB} is exactly equal

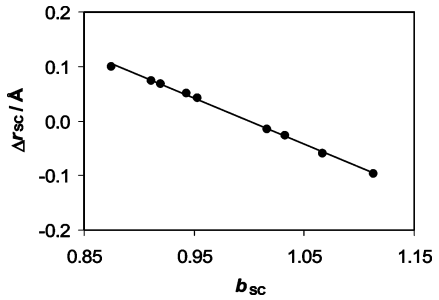

Figure 2. Plot of S−C bond length variation vs natural bond order for the $DMSO_n$ molecules.

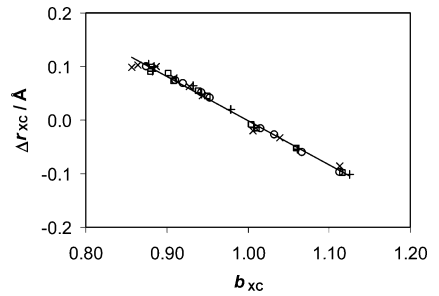

Figure 3. Plot of X−C bond length variation vs natural bond order for $DMSO_n$ (circles), $DMSeO_n$ (squares), $DMTeO_n$ (pluses), $DMPoO_n$ (crosses) and their anions.

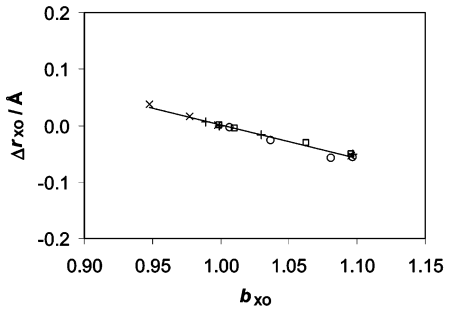

Figure 4. Plot of X−O bond length variation vs natural bond order for $DMSO_n$ (circles), $DMSeO_n$ (squares), $DMTeO_n$ (pluses), $DMPoO_n$ (crosses) and their anions.

to the number of A−B bonds of the Lewis structure. For the S-containing molecules, the Lewis structures have S−C single bonds. Idealized lengths for $b_{SC} = 1$ can therefore be interpolated from the linear fits of Figure 1, yielding $r_{SC}^{(Lewis)}$ values of 1.844, 1.799, and 1.743 Å for the DMS, DMSO, and $DMSO_2$ systems, respectively. The decrease in these idealized bond lengths with increasing coordination of the central S atom is consistent with Bent's Rule,[20] that s character in the S−C bonds increases as p character shifts from these bonds into the hybrids that S directs toward the more electronegative O atoms. Bond length variations $\Delta r_{AB}^{(non-Lewis)}$ can be evaluated using eq 6. For example, DMS^- has equilibrium S−C bond lengths of 1.747 and 1.912 Å which, relative to an idealized length of 1.844 Å, yields $\Delta r_{SC}^{(non-Lewis)}$ values of −0.097 and +0.068 Å, respectively. In Figure 2, we plot $\Delta r_{SC}^{(non-Lewis)}$ vs b_{SC} for the S-containing molecules. The plot clearly reveals a near-linear relationship between bond length variation and the natural bond order. Similar plots resulted for the Se-, Te-, and Po-containing molecules (data not shown).

Figures 3 and 4 are composite plots of the X−C and X−O bond length variations vs bond order for all molecules considered here. Changes in the bond lengths to the central atom resulting from deprotonation correlate well with natural bond

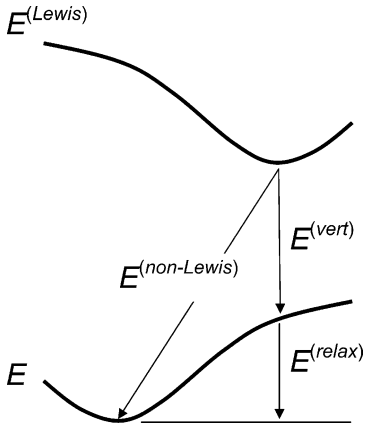

Figure 5. Energy surfaces showing the relationship between the B3LYP energy, E, the localized Lewis energy, $E^{(\mathrm{Lewis})}$, and the adiabatic non-Lewis energy, $E^{(\mathrm{non-Lewis})}$. Note that the latter includes contributions from electronic, $E^{(\mathrm{vert})}$, and geometry, $E^{(\mathrm{relax})}$, relaxation.

order. Thus, NRT clearly suggests that the bond length changes observed in the $DMXO_n$ molecules upon deprotonation are consistent with a resonance-based description of molecular structure.

V. Resonance and Acidity Trend

We further seek to determine whether resonance can likewise account for the acidity trends apparent in the calculated deprotonation energies. The approach we employ to address this issue involves the reevaluation of deprotonation energies using a set of idealized $DMXO_n$ molecules and anions that are fully localized and thereby exhibit no resonance stabilization. NBO energetic analysis is applied to each molecule or anion, calculating the energy of a localized electron density that corresponds directly to the leading resonance form of the hybrids shown in Tables 3 and 4. If resonance, in fact, is largely responsible for the calculated acidity trends of Table 2, this set of ideally localized molecules should reveal substantially diminished trends reflected by weakly varying ΔE values.

It is convenient to consider the partitioning of the B3LYP energy, E, into Lewis and non-Lewis (resonance) contributions

$$E = E^{(\mathrm{Lewis})} + E^{(\mathrm{non-Lewis})} \tag{7}$$

$E^{(\mathrm{Lewis})}$ is the energy of the localized density evaluated by NBO energetic analysis. We choose the energies E and $E^{(\mathrm{Lewis})}$ to be those of the equilibrium structures of the respective B3LYP and localized energy surfaces, as shown in Figure 5. The non-Lewis energy, $E^{(\mathrm{non-Lewis})}$, therefore corresponds to the adiabatic delocalization energy, which includes vertical delocalization $E^{(\mathrm{vert})}$ and geometry relaxation $E^{(\mathrm{relax})}$ energy components. Deprotonation energies are likewise partitioned into Lewis and non-Lewis contributions

$$\Delta E = \Delta E^{(\mathrm{Lewis})} + \Delta E^{(\mathrm{non-Lewis})} \tag{8}$$

where, for example, $\Delta E^{(\mathrm{Lewis})}$ is the energy difference for the reaction of eq 1 based on the $E^{(\mathrm{Lewis})}$ values of eq 7. Importantly, $\Delta E^{(\mathrm{Lewis})}$ represents the deprotonation energy in the absence of resonance effects. The Lewis and non-Lewis components of the deprotonation energies were evaluated and are reported in Table 6.

Figure 6 shows a plot of the ΔE and $\Delta E^{(\mathrm{Lewis})}$ deprotonation energies for the $DMSO_n$ molecules. The (localized) Lewis energies clearly exhibit a stronger acidity trend than the (delocalized) B3LYP values. Whereas the B3LYP trend shows

TABLE 6: Analysis of the Gas-Phase Deprotonation Energies (in kcal/mol) of $DMXO_n$[a]

	ΔE	$\Delta E^{(\mathrm{Lewis})}$	$\Delta E^{(\mathrm{non-Lewis})}$
DMS	400	413	−13
DMSe	397	410	−12
DMTe	393	405	−12
DMPo	393	404	−11
DMSO	382	386	−4
DMSeO	381	385	−4
DMTeO	379	381	−2
DMPoO	381	382	−2
$DMSO_2$	373	361	12
$DMSeO_2$	366	353	14
$DMTeO_2$	360	350	10
$DMPoO_2$	356	341	16

[a] B3LYP/aVDZ values. See eq 8.

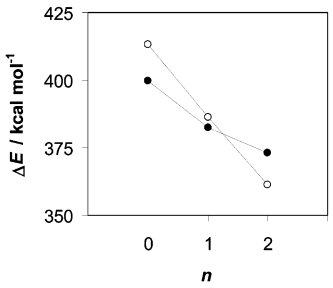

Figure 6. Plot of the deprotonation energies of the $DMSO_n$ molecules. The filled and unfilled circles respectively correspond to the delocalized ΔE and localized $E^{(\mathrm{Lewis})}$ values of eq 8.

a 37 kcal/mol decrease in deprotonation energy, from 400 kcal/mol for DMS to 373 kcal/mol for $DMSO_2$, the Lewis energies reveal a 52 kcal/mol decrease, from 413 to 361 kcal/mol. These results clearly suggest that non-Lewis effects enhance the acidity of DMS, decreasing its deprotonation energy by 13 kcal/mol ($\Delta E^{(\mathrm{non-Lewis})}$ in Table 6). This effect is principally due to the resonance stabilization (particularly the $n_C \rightarrow \sigma^*_{SC}$ interaction) of DMS^-. Interestingly, however, non-Lewis effects weaken the acidity of $DMSO_2$, increasing its deprotonation energy by 12 kcal/mol. Resonance stabilizes $DMSO_2$ more strongly than its anion, a result largely consistent with the strong resonance mixing seen in both $DMSO_2$ and $DMSO_2^-$ hybrids of Tables 3 and 4. These results clearly suggest that resonance is not the origin of the enhanced acidity of the $DMXO_n$ molecules with increasing coordination of the central atom.

VI. Conclusions

The gas-phase acidities of DMS, DMSO, and $DMSO_2$ increase with the increasing coordination of the central S atom, a trend that is evident from the decreasing deprotonation energies (B3LYP/aVDZ) of 400, 382, and 373 kcal/mol, respectively. The conventional resonance delocalization description of this trend suggests that the enhanced acidity of $DMSO_2$ relative to DMS results from the stronger charge delocalization of the $DMSO_2^-$ anion compared to that of DMS^-. Natural resonance theory (NRT) indeed reveals important $n_C \rightarrow \sigma^*$ interactions that delocalize $DMSO_2^-$ somewhat more strongly than DMS^-. However, our analysis also shows that $DMSO_2$ itself is strongly delocalized, by $n_O \rightarrow \sigma^*$ interactions. In fact, $DMSO_2$ is somewhat more strongly delocalized than its anion, so that resonance favors $DMSO_2$ over its anion and increases the deprotonation energy by an estimated 12 kcal/mol. In contrast, DMS is highly localized. Resonance therefore favors DMS^- over DMS, decreasing the deprotonation energy of DMS by

roughly 13 kcal/mol. Similar effects are calculated for the group 16 congeners $DMXO_n$ (X = Se, Te, Po and $n = 0-2$). These results lead one to conclude that resonance is not responsible for the acidity trend. The acidity trend apparently stems from other factors, such as the electrical stabilization of the anionic carbon center adjacent to polarized sulfenyl (RS), sulfinyl (RSO), and sulfonyl (RSO_2) groups. The methods employed here, however, do not provide a quantitative assessment of these factors.

Resonance does account for the structural changes that the $DMXO_n$ molecules undergo on deprotonation. NRT was used to evaluate bond orders for these molecules and their anions. Importantly, a nearly linear relationship is observed between the calculated bond orders and the bond length variations.

Acknowledgment. Portions of this work were completed on a high performance computer administered by the Office of Information Technology at Indiana State University.

References and Notes

(1) Wiberg, K. B.; Castejon, H. *J. Am. Chem. Soc.* **1994**, *116*, 10489.

(2) Speers, P.; Laidig, K. E.; Streitwieser, A. *J. Am. Chem. Soc.* **1994**, *116*, 9257.

(3) Streitwieser, A., Jr.; Williams, J. E., Jr. *J. Am. Chem. Soc.* **1975**, *97*, 191.

(4) Lehn, J.-M.; Wipff, G. *J. Am. Chem. Soc.* **1976**, *98*, 7498.

(5) Hopkinson, A. C.; Lien, M. H. *J. Org. Chem.* **1980**, *46*, 998.

(6) Larson, J. R.; Epiotis, N. D. *J. Am. Chem. Soc.* **1981**, *103*, 410.

(7) Schleyer, P. v. R.; Clark, T.; Kos, A. J.; Spitznagel, G. W.; Rohde, C.; Arad, D.; Houk, K. N.; Rondan, N. G. *J. Am. Chem. Soc.* **1984**, *106*, 6467.

(8) Bors, D. A.; Streitwieser, A., Jr. *J. Am. Chem. Soc.* **1986**, *108*, 1397.

(9) Bader, R. F. W. *Atoms in Molecules: A Quantum Theory*; Oxford University Press: New York, 1990.

(10) (a) Glendening, E. D.; Badenhoop, J. K.; Reed, A. E.; Carpenter, J. E.; Bohmann, J. A.; Morales, C. M.; Weinhold, F. *NBO 5.0*; Theoretical Chemistry Institute, University of Wisconsin: Madison, WI, 2001. (b) Reed, A. E.; Curtiss, L. A.; Weinhold, F. *Chem. Rev.* **1988**, *88*, 899. (c) Reed, A. E.; Weinhold, F. *J. Chem. Phys.* **1985**, *83*, 1736. (d) Reed, A. E.; Weinhold, F. *J. Chem. Phys.* **1983**, *78*, 4066.

(11) (a) Glendening, E. D.; Weinhold, F. *J. Comput. Chem.* **1998**, *19*, 593. (b) Glendening, E. D.; Weinhold, F. *J. Comput. Chem.* **1998**, *19*, 610. (c) Glendening, E. D.; Badenhoop, J. K.; Weinhold, F. *J. Comput. Chem.* **1998**, *19*, 628.

(12) Frisch, M. J.; Trucks, G. W.; Schlegel, H. B.; Scuseria, G. E.; Robb, M. A.; Cheeseman, J. R.; Zakrzewski, V. G.; Montgomery, J. A., Jr.; Stratmann, R. E.; Burant, J. C.; Dapprich, S.; Millam, J. M.; Daniels, A. D.; Kudin, K. N.; Strain, M. C.; Farkas, O.; Tomasi, J.; Barone, V.; Cossi, M.; Cammi, R.; Mennucci, B.; Pomelli, C.; Adamo, C.; Clifford, S.; Ochterski, J.; Petersson, G. A.; Ayala, P. Y.; Cui, Q.; Morokuma, K.; Malick, D. K.; Rabuck, A. D.; Raghavachari, K.; Foresman, J. B.; Cioslowski, J.; Ortiz, J. V.; Stefanov, B. B.; Liu, G.; Liashenko, A.; Piskorz, P.; Komaromi, I.; Gomperts, R.; Martin, R. L.; Fox, D. J.; Keith, T.; Al-Laham, M. A.; Peng, C. Y.; Nanayakkara, A.; Gonzalez, C.; Challacombe, M.; Gill, P. M. W.; Johnson, B. G.; Chen, W.; Wong, M. W.; Andres, J. L.; Head-Gordon, M.; Replogle, E. S.; Pople, J. A. *Gaussian 98*, revision A.7; Gaussian, Inc.: Pittsburgh, PA, 1998.

(13) (a) Becke, A. D. *J. Chem. Phys.* **1993**, *98*, 5648. (b) Lee, C.; Yang, W.; Parr, R. G. *Phys. Rev. B* **1988**, *37*, 785. (c) Vosko, S. H.; Wilk, L.; Nusair, M. *Can. J. Phys.* **1980**, *58*, 1200. (d) Stephens, P. J.; Devlin, F. J.; Chabalowski, C. F.; Frisch, M. J. *J. Phys. Chem.* **1994**, *98*, 11623.

(14) (a) Dunning, T. H., Jr. *J. Chem. Phys.* **1989**, *90*, 1007. (b) Kendall, R. A.; Dunning, T. H., Jr.; Harrison, R. J. *J. Chem. Phys.* **1992**, *96*, 6796.

(15) (a) Peterson, K. A. *J. Chem. Phys.* **2003**, *119*, 11099. (b) Peterson, K. A.; Figgen, D.; Goll, E.; Stoll, H.; Dolg, M. *J. Chem. Phys.* **2003**, *119*, 11113.

(16) (a) MOLPRO is a package of ab initio programs written by H.-J. Werner and P. J. Knowles with contributions from J. Almlof, R. D. Amos, A. Berning, D. L. Cooper, M. J. O. Deegan, A. J. Dobblyn, F. Eckert, S. T. Elbert, C. Hampel, R. Lindh, A. W. Lloyd, W. Meyer, A. Nicklass, K. Peterson, R. Pitzer, A. J. Stone, P. R. Taylor, M. E. Mura, P. Pulay, M. Schutz, H. Stoll, and T. Thorsteinsson. (b) Hampel, C.; Peterson, K.; Werner, H.-J. *Chem. Phys. Lett.* **1992**, *190*, 1. (c) Knowles, P. J.; Hampel, C.; Werner, H.-J. *J. Chem. Phys.* **1993**, *99*, 5219.

(17) (a) Peterson, K. A.; Woon, D. E.; Dunning, T. H., Jr. *J. Chem. Phys.* **1994**, *100*, 7410. (b) Woon, D. E.; Dunning, T. H., Jr. *J. Chem. Phys.* **1994**, *101*, 8877.

(18) Ingemann, S.; Nibbering, N. M. M. *Can. J. Chem.* **1985**, *62*, 2273.

(19) Cumming, J. B.; Kebarle, P. *Can. J. Chem.* **1978**, *56*, 1.

(20) Bent, H. A. *Chem. Rev.* **1961**, *61*, 275.